Yang *et al. Molecular Cancer* (2025) 24:158
https://doi.org/10.1186/s12943-025-02354-2

Molecular Cancer

RESEARCH Open Access

Loss of TACC2 impairs chemokine CCL3 and CCL4 expression and reduces response to anti-PD-1 therapy in soft tissue sarcoma

Jing Yang[1†], Xiuxia Lu[2†], Qiyan Cai[1†], Mengmeng Liu[1,3†], Tianliang Xia[4], Dongchun Hong[5], Liyuan Le[1], Xinke Zhang[6] and Xing Zhang[1*]

Abstract

Background Soft tissue sarcoma (STS) is a rare, heterogeneous malignancy with limited treatment options for metastatic disease. Despite advances in immunotherapy, including PD-1 inhibitors, clinical outcomes remain suboptimal, highlighting the need for novel biomarkers and therapeutic strategies. This study investigated the role of TACC2 in STS, focusing on its impact on the immune microenvironment and immunotherapy response.

Methods Whole-exome sequencing was performed to characterize TACC2-related genomic alterations in STS cohorts, complemented by immunohistochemistry for protein-level validation. Mechanistic insights were obtained through chromatin immunoprecipitation (ChIP) and co-immunoprecipitation assays, focusing on TACC2's interaction with the NuRD/CoREST complex. The efficacy of anti-PD-1 therapy was evaluated in TACC2-overexpressing mouse models, and clinical relevance was analyzed using patient survival and treatment response data.

Results TACC2 acted as a tumor suppressor in STS, with low expression associated with poor overall survival. Mechanistically, TACC2 enhanced CCL3 and CCL4 transcription, promoting CD8 + T cell infiltration by inhibiting NuRD/CoREST nuclear translocation. In vivo, TACC2 overexpression synergized with PD-1 blockade therapy, leading to a significant reduction in tumor volume and prolonged survival. Clinically, high TACC2 expression was associated with improved responses to immunotherapy.

Conclusions In conclusion, TACC2 is an important regulator of the immune response in STS, functioning as a tumor suppressor and a modulator of response to PD-1 blockade. Its role in modulating chemokine expression and CD8 + T cell infiltration highlights its potential as a therapeutic target and predictive biomarker for STS immunotherapy.

†Jing Yang, Xiuxia Lu, Qiyan Cai, Mengmeng Liu and Tianliang Xia, equally contributed to this work.

*Correspondence:
Xing Zhang
zhangxing@sysucc.org.cn

Full list of author information is available at the end of the article

Graphical abstract

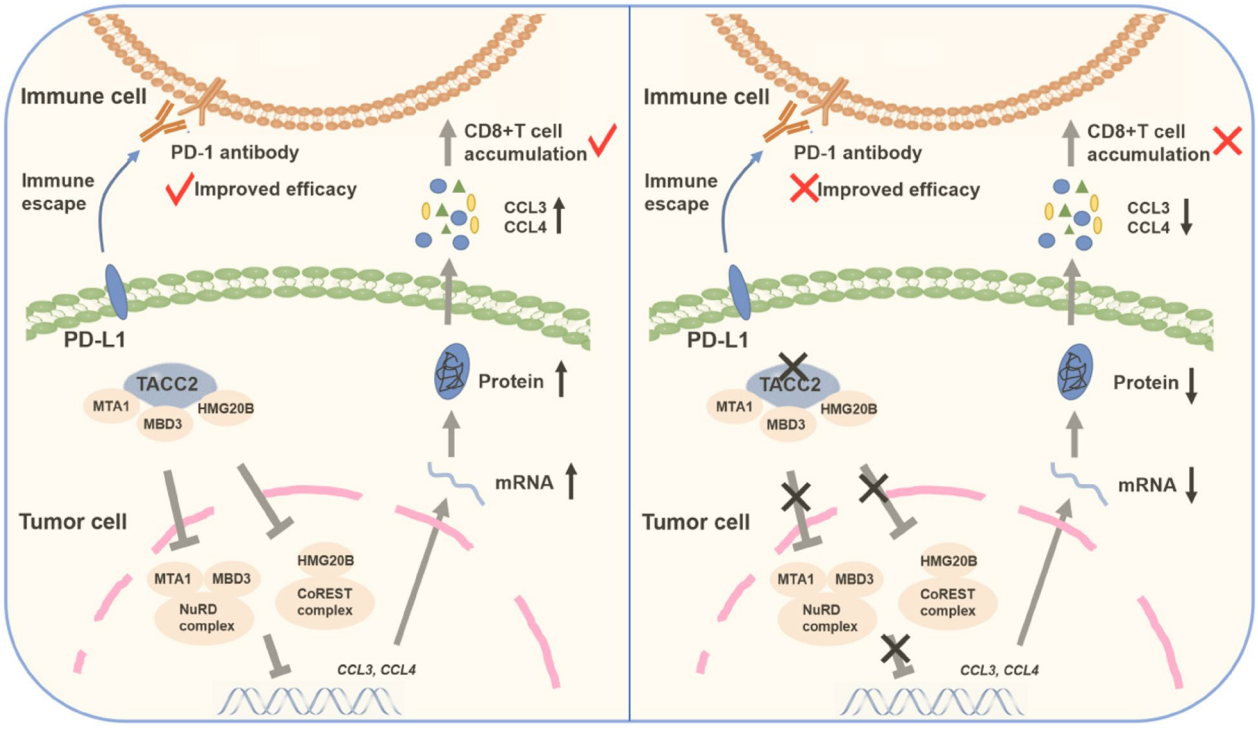

Keywords Soft tissue sarcoma, TACC2, PD-1 Blockade, Chromatin remodeling, Tumor suppressor, Immune microenvironment

Background

Soft tissue sarcoma (STS) represents a heterogeneous and relatively rare group of malignancies arising from mesenchymal tissues, with an incidence of fewer than 6 cases per 100,000 individuals annually [1]. Despite accounting for no more than 1% of all adult malignancies and 15% of pediatric malignancies, the incidence of STS has been rising in recent years [2, 3]. STS accounts for over 80% of all sarcomas, and more than 50 subtypes have been defined, with common subtypes including undifferentiated pleomorphic sarcoma, liposarcoma, synovial sarcoma, and fibrosarcoma [1, 2, 4]. The current standard treatment for STS involves a multidisciplinary approach, with surgical resection as the cornerstone for localized, clinically resectable cases [5]. However, for unresectable or metastatic STS, effective systemic therapies are limited, with palliative chemotherapy as the primary treatment option and a median survival of less than two years [5–8].

In recent years, antibodies targeting programmed death-1 (PD-1) and its ligand programmed death ligand-1 (PD-L1) have made significant breakthroughs in cancer treatment. While anti-PD-1 antibody monotherapy has shown significant efficacy in Hodgkin lymphoma, cutaneous squamous cell carcinoma, and melanoma, its effectiveness in most other cancers, including STS, remains limited, with response rates below 20% [9, 10]. Certain STS histologies, such as alveolar soft part sarcoma and undifferentiated pleomorphic sarcoma, have shown greater clinical activity in response to anti-PD-1 antibodies [9, 11]. Accordingly, the National Comprehensive Cancer Network (NCCN) guidelines have recommended anti-PD-1 antibodies for the treatment of certain STS subtypes. However, most STS cases fail to respond to anti-PD-1 therapy, and conventional biomarkers for predicting ICI response, including tumor mutational burden and PD-L1 expression, do not reliably identify the majority of responders in STS [12]. These observations underscore an urgent need for novel therapeutic approaches and reliable prognostic biomarkers to improve clinical outcomes for STS patients.

Tumor suppressor genes play a crucial role in the prevention, early diagnosis, treatment, and prognosis of malignancies. Discovering new tumor suppressor genes could provide promising strategies for precision oncology [13]. Several well-known tumor suppressor genes, such as p53, ATRX, Rb, p16, and PTEN, have been implicated in tumorigenesis due to mutations or deletions [14–17]. However, research into tumor suppressor genes specific

to STS remains limited. Transforming acidic coiled-coil proteins (TACCs), including TACC1, TACC2, and TACC3, are involved in stabilizing the mitotic spindle and promoting microtubule formation during cell mitosis, which is critical for maintaining genetic stability [18]. Dysregulation of TACC proteins can disrupt chromatin remodeling complex interactions, reducing genomic stability and promoting tumorigenesis [19]. TACC2, also known as AZU-1, was initially identified as a tumor suppressor gene in breast cancer but has also been shown to have tumor-promoting effects in prostate and liver cancers [20–22]. The role of TACC2 in STS, however, remains poorly understood.

In this study, we investigated the role of TACC2 in STS and demonstrated its role as a tumor suppressor. Our findings reveal that TACC2 enhances anti-tumor immunity through transcriptional upregulation of the chemokines CCL3 and CCL4. Furthermore, TACC2 may serve as a predictive biomarker for the efficacy of anti-PD-1 therapy. Mechanistically, TACC2 interacts with MTA1, MBD3, and HMG20B, inhibiting the formation of HDAC corepressor complexes. This epigenetic regulation leads to the transcriptional activation of CCL3 and CCL4, which promotes the recruitment of CD8 + T cells to the tumor microenvironment, thereby improving the immune response and enhancing the efficacy of anti-PD-1 therapy.

Methods

Tissue samples

Fresh frozen tissues and pathological sections were collected from the Sun Yat-Sen University Cancer Center (SYSUCC). Written informed consent for collection and publication of medical information was obtained from each patient during their first visit to the center. The study was conducted in accordance with the ethical guidelines, and all procedures were approved by the Institutional Review Board (IRB) of SYSUCC. Tumor tissues and adjacent non-tumor tissues were collected from surgical specimens of STS patients. All samples were pathologically confirmed, with adjacent non-tumor tissues verified to be free of tumor infiltration.

Cell culture

STS cell lines HT1080, U2197, SK-LMS, SW982, GP2-293, and 293T were cultured in DMEM supplemented with 10% fetal bovine serum (FBS). MCA205 cells were cultured in RPMI 1640 supplemented with 10% FBS. All cells were maintained in a humidified atmosphere containing 5% CO2 at 37 °C.

Whole-Exome sequencing and copy-number variation analysis

Tumor DNA from FFPE samples was extracted using the Maxwell 16 FFPE Plus LEV DNA Purification Kit (Promega-AS1135), while genomic DNA from blood was purified using the OMEGA Blood DNA Kit according to the manufacturer's protocol. DNA was fragmented to an appropriate size for library construction, followed by library preparation using the Agilent SureSelect Human All Exon V6 Kit. For FFPE samples with total DNA < 200 ng, libraries were constructed using the KAPA Hyper Prep Kit. Targeted DNA fragments were captured and sequenced on the Illumina NovaSeq 6000 platform. Base calls and fluorescence intensities were processed into fastq files. Copy-number variation (CNV) analysis was performed using CNVkit, with matched tumor-normal BAM files as input. Copy-number gain was defined as an increase in the number of gene copies by one, while amplification referred to an increase of multiple copies in a specific genomic region. Conversely, copy-number loss was defined as a single-copy decrease, whereas deletion represented the loss of multiple copies in a given region.

Chemokine array analysis

Chemokine protein array membranes (RayBiotech®, Inc.) were blocked with 5% BSA in PBS for 1 h at room temperature, followed by overnight incubation at 4 °C with 8× concentrated supernatants from tumor cells. After extensive washing to remove unbound materials, the membranes were incubated with biotin-conjugated antibodies (1:1000 dilution) for 2 h at room temperature. Following three additional washes, the membranes were incubated with HRP-conjugated streptavidin for 2 h at room temperature. Signal intensities were quantified using the ImageQuant LAS4000 system (GE Healthcare Corporate), and fold changes in protein expression were calculated.

RNA-seq and immune cell infiltration analysis

Total RNA was extracted using TRIzol™ reagent (ThermoFisher #15596018CN). RNA-Seq libraries were prepared and sequenced on an Illumina platform at the Berry Genomics Corporation (Beijing, China). Differentially expressed genes were identified using DESeq2. Single-sample Gene Set Enrichment Analysis (ssGSEA) was performed to assess the relative infiltration of immune cells within the tumor microenvironment.

Immunohistochemistry staining

Immunohistochemistry (IHC) staining was performed on paraffin-embedded tissue sections. After deparaffinization and rehydration, endogenous peroxidase activity was blocked with 3% hydrogen peroxide, antigen retrieval was conducted using EDTA buffer, and non-specific binding

was blocked with normal serum. Tissue sections were incubated with primary antibodies at 4 °C overnight, followed by incubation with secondary antibodies and visualization using DAB substrate. Counterstaining was performed with hematoxylin to visualize nuclei. The antibodies used included anti-TACC2 (11407-1-AP, Proteintech), anti-Ki-67 (ab16667, Abcam), anti-CD4 (ab183685, Abcam), anti-CD8 (ab209775, Abcam), and anti-CD11b (ab133357, Abcam), along with goat anti-rabbit (PV-6001, ZSGB-BIO) and goat anti-mouse (PV-6002, ZSGB-BIO) secondary antibodies.

Quantitative real-time PCR

Total RNA was extracted from tissues and cells using the TRIzol™ reagent (Sigma-Aldrich), and cDNAs were synthesized with the A0010CG Color Reverse Transcription Kit (EZBioscience, China) according to the manufacturer's protocol. Quantitative real-time PCR (qRT-PCR) was performed using SYBR Green Master Mix (EZBioscience) on a Bio-Rad CFX96 PCR instrument. GAPDH was used as the internal control for normalizing the target gene expression levels. The relative mRNA expression was calculated with the formula 2[−(delta delta Ct)]. All primers used are listed in Supplementary Table 2.

Plasmid construction and stable cell line establishment

The full-length coding sequence (CDS) region of TACC2 was PCR-amplified and cloned into the pEGFP-C2 vector (EcoRI/BamHI) to generate the EGFP-TACC2 overexpression plasmid. For the tetracycline (dox)-inducible system, the EGFP-TACC2 was cloned into the pRetroX-TRE3G vector via EcoRI/BamHI. shRNA plasmids targeting TACC2 (sh-TACC2) and a scrambled control (sh-ctrl) were designed, synthesized, and inserted into the pLKO.1 vector. All constructs were verified by DNA sequencing. For lentiviral production, HEK-293T or GP2-293 cells were transfected with plasmids using Lipofectamine 3000. Viral supernatants were collected after 48 h, filtered (0.45 μm), and stored at − 80 °C. Target cells were infected twice with viral particles and selected with puromycin or G418 for 72 h. Stable overexpression or knockdown was confirmed by Western blot.

SiRNA transfection

The specific siRNAs and a scrambled control siRNA were purchased from Guangzhou RiboBio Co., Ltd. Cells were transfected with siRNAs using Lipofectamine RNAiMAX (Invitrogen) according to the manufacturer's protocol. The efficiency of gene knockdown was confirmed by qRT-PCR and Western blot 48 h post-transfection. Sequences of the siRNAs are provided in Supplementary Table 3.

MTT and colony formation

For the MTT assay, cells were seeded into 96-well plates, and 20 μL of 5 mg/mL MTT solution (Sigma-Aldrich) was added to each well. After 4 h of incubation at 37 °C, the medium was removed, and 200 μL of DMSO was added to dissolve the formazan crystals. Absorbance was measured at 490 nm using a microplate reader. For the colony formation assay, cells were seeded into 6-well plates at a density of 500 cells per well. After 10–14 days, colonies were fixed with 4% paraformaldehyde for 15 min, stained with 0.5% crystal violet for 15 min, and counted.

Cell cycle analysis

Harvested cells were washed twice with PBS and fixed overnight in ice-cold 70% ethanol at − 20 °C. After centrifugation, cells were washed with PBS and stained with a DNA staining solution containing 50 μg/mL propidium iodide (PI; Sigma-Aldrich, #P4864), 100 μg/mL RNase A (Thermo Fisher, #EN0531), and 0.1% Triton X-100. Cells were incubated in the dark at 37 °C for 30 min. Cell cycle distribution was analyzed using an ACEA NovoCyte instrument. Data were processed using ACEA NovoCyte software to quantify G0/G1, S, and G2/M phases.

Western blot and Immunoprecipitation analysis

Proteins were extracted using RIPA buffer supplemented with protease inhibitors and quantified using Pierce® BCA Protein Assay Kit (23227, Thermo Scientific) following manufacturer's instructions. Protein samples were separated by SDS-PAGE and transferred to polyvinylidene fluoride (PVDF) membranes. The membranes were blocked with 5% non-fat milk and incubated with primary antibodies against TACC2, HMG20B, HDAC1, MTA1, MBD3, β-actin, or GAPDH overnight at 4 °C. Following incubation with secondary antibodies for 1 h at room temperature, bands were visualized using ECL substrate. For immunoprecipitation, cell lysates were incubated with specific antibodies and Protein A/G agarose beads, followed by Western blot analysis of the immunoprecipitated complexes. Antibodies included: anti-TACC2 (11407-1-AP, Proteintech), anti-HMG20B (14582-1-AP, Proteintech), anti-HDAC1 (#34589, CST), anti-MTA1 (#5646, CST), anti-MTA2 (66195-1-Ig, Proteintech), anti-MBD3 (14258-1-AP, Proteintech), anti-GAPDH (97166 S, CST), and anti-β-actin (3700 S, CST).

Flow cytometry

Tissues were finely chopped into small fragments and digested with 0.2 mg/mL collagenase IV and 0.1 mg/mL DNase I at 37 °C for 2 h. After digestion, the suspensions were passed through a 70 μm strainer, and red blood cell lysis buffer was added to lyse red blood cells. Cells were then stained with fluorophore-conjugated

antibodies (1:100 dilution in PBS) for 30 min at 4 °C under light-protected conditions. The antibody panel included: anti-CD3 (APC/Cy7, BioLegend #100330; PE/Cyanine7, BioLegend #100220) for pan-T cell identification; anti-CD8α (PerCP-Cyanine5.5, eBioscience #45-0081-82) for cytotoxic T cells; anti-CD4 (Brilliant Violet 510™, BioLegend #100559) for CD4 + T cells; anti-CD19 (PerCP/Cy5.5, BioLegend #115534) for B lymphocytes; anti-NK1.1 (Alexa Fluor 700 eBioscience #56-5941-82) for NKT cells; and macrophage markers including anti-CD206 (BV650, BioLegend #141723), anti-CD11b (PE, BioLegend #101208), and anti-F4/80 (BV785, BioLegend #123141). Cells were subsequently washed twice with ice-cold PBS. Flow cytometry analysis was performed using a Beckman Coulter Gallios Flow Cytometer, and data were analyzed using CytExpert software.

Enzyme-linked immunosorbent assay

The levels of chemokines CCL3 and CCL4 in cell culture supernatants and serum samples were measured using enzyme-linked immunosorbent assay (ELISA) kits (88-7035-22 and 88-7034-22, Invitrogen) according to the manufacturer's instructions. Absorbance was read at 450 nm using an ELX 800 96-well plate reader (BioTek, VT, USA).

Chromatin Immunoprecipitation (ChIP) assays

HT1080 cells transfected with either sh-ctrl or sh-TACC2 were cultured in 15 cm dishes. When cell density reached 80–90%, the cells were cross-linked with 1% formaldehyde, washed with PBS, scraped in PBS and then lysed with lysis buffer. The genomic DNA was sonicated utilizing ultrasonicator (Covaris E220) to generate approximately 500-bp fragments within the lysis buffer. Following the removal of debris, the supernatants were diluted, and the lysates were incubated with a specific antibody (rabbit IgG, CST #2729S; anti-H3K27ac, CST #8173S; anti-H4K16ac, CST #13534S) overnight at 4℃. Protein-DNA complexes were captured by adding pre-blocked Protein A agarose beads, followed by extensive washing to remove nonspecific bindings. Protein-DNA complexes were eluted from the beads and subjected to reverse cross-linking. DNA was then purified using the Qiagen PCR purification kit according to the manufacturer's protocol. Purified DNA was subjected to a qPCR analysis using ChamQ SYBR® qPCR Master Mix (EZBioscience) on a LightCycler. PCR conditions were set according to the instructions provided in SYBR Green Kit (Roche). Primer sequences used for ChIP-qPCR are listed in Supplementary Table 4.

Chemotaxis assay

Peripheral blood mononuclear cells (PBMCs) were isolated from peripheral blood obtained from healthy donors using Ficoll density gradient centrifugation. CD8 + T cells and CD4 + T cells were purified from PBMCs via positive selection using anti-CD8 and anti-CD4 MicroBeads kit (Miltenyi Biotec, #130-045-201 and #130-045-101) following the manufacturer's instructions. Chemotaxis assays were conducted using 24-well Transwell plates with 5-μm pore polycarbonate membranes (Corning, #3421). A total of 5×10^5 PBMCs, CD8 + T or CD4 + T cells in serum-free medium were placed in the upper chamber. The lower chamber was filled with 0.1% FBS RPMI-1640 medium (negative control) or supernatant from tumor cells (48 h) supplemented with or without human CCL3 (100 ng/mL; PeproTech, #300-06) and CCL4 (100 ng/mL; PeproTech, #300-07). After 6–8 h of incubation at 37 °C in 5% CO_2, cells migrating to the bottom chamber were collected and counted. Each condition was tested in triplicate.

Animal experiments

All experimental procedures were approved by the Institutional Animal Care and Use Committee of Sun Yat-Sen University, Guangzhou, China. C57BL/6 mice, purchased from the Guangdong Medical Laboratory Animal Center, were subcutaneously injected with 5×10^5 MCA205 cells. Tumor growth was monitored every three days, and tumor volumes were calculated using the formula: 0.52 × length × width^2. Mice were orally administered doxycycline to induce TACC2 expression. Anti-PD-1 antibody (BioXcell, #BP0146) was administered intraperitoneally at a dose of 10 mg/kg every three days. At the end of the experiments, tumors were excised, weighed, and processed for further analysis.

Statistical analysis

All data were presented as mean ± standard deviation (SD) or standard error of the mean (SEM). Statistical significance was determined using Student's t-test or one-way ANOVA. Survival curves were analyzed using the Kaplan-Meier method and compared by the log-rank test. A p-value < 0.05 was considered statistically significant. R (v4.0.3), GraphPad Prism (v8.0) and SPSS (v19.0) were used to analyze and visualize the data.

Results

TACC2 expression and copy number variation in soft tissue sarcoma

We analyzed WES data from 41 STS cases, comprising various histological subtypes: leiomyosarcoma ($n = 5$), rhabdomyosarcoma ($n = 6$), alveolar soft part sarcoma ($n = 7$), synovial sarcoma ($n = 7$), undifferentiated pleomorphic sarcoma ($n = 4$), fibrosarcoma ($n = 2$), malignant peripheral nerve sheath tumor ($n = 2$), and others ($n = 8$). As shown in Figs. 1A and 25 cases (60.98%) exhibited TACC2 copy number loss, 10 (24.39%) had no detectable

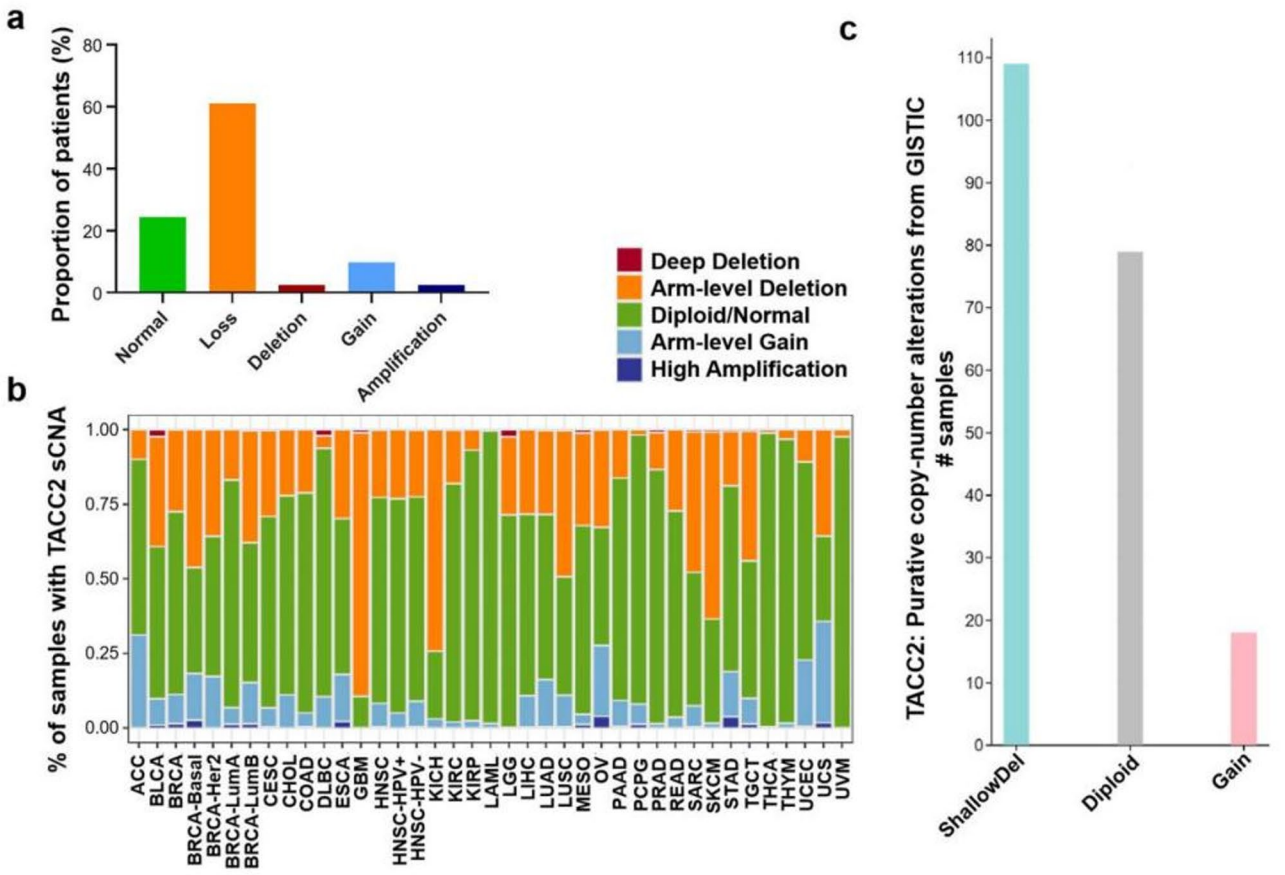

Fig. 1 Frequent loss of TACC2 gene copy number in soft tissue sarcomas. **a**. Whole-exome sequencing was performed on 41 specimens and gene copy number alterations were assessed. Loss or deletion of TACC2 was observed in 63.4% of cases, which was significantly more frequent than copy number gain or amplification (12.2%). **b**. TACC2 copy number alterations were further analyzed using patient datasets from The Cancer Genome Atlas (TCGA) (http://timer.comp-genomics.org/). Deletions in the TACC2 gene were significantly more prevalent than copy number gains. Color codes: red, deep deletion; orange, arm-level deletion; green, diploid/normal; light blue, arm-level gain; dark blue, high amplification. **c**. TACC2 copy number alterations in 206 soft tissue sarcoma patients from the TCGA dataset were analyzed (http://timer.comp-genomics.org/). Color codes: blue, shallow deletion; gray, diploid; red, gain

variation, 1 (2.44%) had a deletion, 4 (9.76%) showed a slight gain, and 1 (2.44%) had amplification.

Additionally, our analysis of the TCGA pan-cancer database revealed that in various malignancies, including STS, the frequency of TACC2 gene deletions was significantly higher than that of copy number gains (Fig. 1B). Specifically, in 206 STS cases (histological subtypes: leiomyosarcoma = 80, synovial sarcoma = 10, myxofibrosarcoma = 17, malignant peripheral nerve sheath tumor = 5, liposarcoma = 50, undifferentiated pleomorphic sarcoma/malignant fibrous histiocytoma/high-grade spindle cell sarcoma = 44), 109 cases (52.9%) had TACC2 copy number loss, whereas only 18 cases (8.7%) had copy number gain (Fig. 1C). Notably, TACC2 copy number loss was observed across nearly all subtypes, though it was less frequent in synovial sarcoma (Supplementary Fig. 1).

We also integrated transcriptomic data from 1191 normal tissue samples (adipose, muscle, and nerve) obtained from the GTEx and TCGA databases, as well as 263 STS samples from the TCGA database.The results indicated that TACC2 expression levels were significantly higher in normal tissues compared to STS tissues ($p < 2.22e\text{-}16$, Fig. 2A). Subtype-specific analyses further revealed reduced TACC2 expression in liposarcoma (vs. adipose tissue, $p < 2.22e\text{-}16$), leiomyosarcoma (vs. muscle tissue, $p < 2.22e\text{-}16$), and malignant peripheral nerve sheath tumor (vs. nerve tissue, $p = 7.9e\text{-}8$), with consistent significance across all comparisons (Supplementary Fig. 2). Moreover, high TACC2 expression was associated with longer overall survival (OS) and progression-free survival (PFS), with p-values of 0.017 and 0.042, respectively (Fig. 2B).

To validate these findings, we collected 9 pairs of STS and their adjacent non-tumor tissues, including 2 cases of fibrosarcoma, 2 cases of undifferentiated pleomorphic sarcoma, 1 case of malignant solitary fibrous tumor, 2 cases of liposarcoma, 1 case of clear cell sarcoma, and 1 case of leiomyosarcoma. All tumor and adjacent

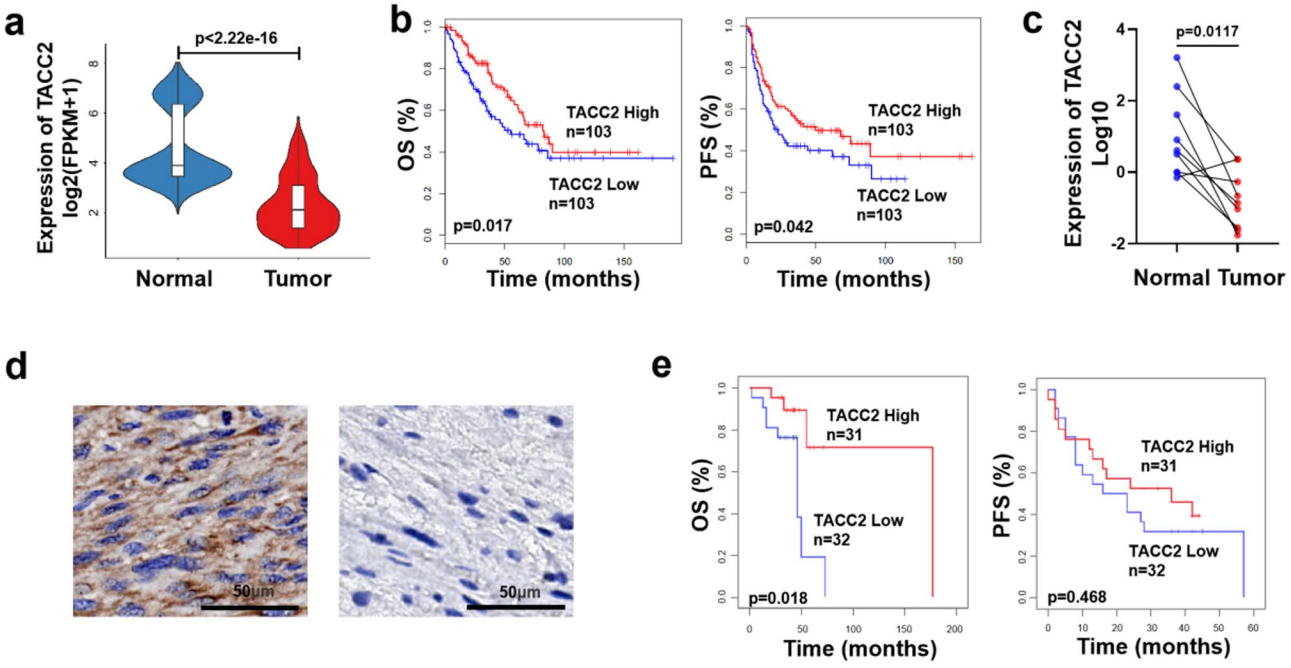

Fig. 2 Prognostic significance of TACC2 expression in soft tissue sarcoma patients. **a**. TACC2 expression levels (log_2[FPKM + 1]) were compared between 1191 normal tissue samples (adipose, muscle, nerve, and uterus) obtained from the GTEx and TCGA databases, as well as 263 soft tissue sarcoma samples from The Cancer Genome Atlas (TCGA). Statistical comparison using the Wilcoxon rank-sum test revealed significantly lower TACC2 expression in sarcomas compared to normal tissues ($p < 2.22 \times 10^{-16}$). **b**. Kaplan–Meier survival analysis based on TCGA data ($n = 206$) demonstrated that lower TACC2 mRNA expression was significantly associated with poorer overall survival (OS) and progression-free survival (PFS). **c**. TACC2 expression levels were measured in nine paired soft tissue sarcoma and adjacent normal tissues. Analysis revealed significantly lower TACC2 expression in sarcomas compared to normal tissues (Wilcoxon signed-rank test, $p = 0.0117$). Data are presented as the mean ± SEM. **d**. Immunohistochemical staining for TACC2 was performed on soft tissue sarcoma samples, with representative images showcasing tissues with low and high TACC2 expression. **e**. TACC2 mRNA expression levels were quantified by quantitative real-time PCR (qRT-PCR) in tumor tissues from 63 sarcoma patients. Based on the median TACC2 mRNA expression level, patients were stratified into low-expression ($n = 32$) and high-expression ($n = 31$) groups. Kaplan–Meier survival analysis demonstrated that high TACC2 expression was significantly associated with improved OS (log-rank test, $p = 0.018$)

non-tumor tissues were obtained from surgical specimens and pathologically confirmed. RNA was extracted, and TACC2 expression was analyzed using qPCR. The results showed that TACC2 expression levels were significantly downregulated in STS tissues compared to adjacent non-tumor tissues (Fig. 2C). Furthermore, IHC staining of STS tissues revealed varying levels of TACC2 expression, with examples of high and low expression shown in Fig. 2D.

We collected frozen tissue samples from 63 STS patients, and clinical characteristics of the patients were shown in Supplementary Table 1. We used qRT-PCR to detect TACC2 expression at the transcript level in these tissues and categorized patients into high and low TACC2 expression groups. Further survival analysis revealed a positive correlation between TACC2 expression levels and OS ($p = 0.018$, Fig. 2E). Although the correlation between TACC2 expression and PFS was not statistically significant ($p = 0.468$), Kaplan-Meier analysis still indicated a trend towards better PFS in patients with higher TACC2 expression.

TACC2 overexpression inhibits STS cell growth in vitro and in vivo

To investigate the effects of TACC2 overexpression and knockdown on cell division, we performed MTT and colony formation assays. In vitro experiments demonstrated that knockdown of TACC2 using siRNA or shRNA led to an increase in proliferation and colony formation (Supplementary Fig. 3). Conversely, TACC2 overexpression significantly inhibited the proliferation and colony formation of STS cell lines (Supplementary Fig. 4). Cell cycle analysis following TACC2 knockdown revealed a significant reduction in the proportion of cells in the G0/G1 phase, indicating accelerated cell cycle progression. In contrast, TACC2 overexpression led to an increased proportion of cells in the G0/G1 phase (Supplementary Fig. 5).

In vivo, C57BL/6 mice were injected with MCA205 cells stably expressing TET-ON TACC2. Mice in the experimental group were orally administered doxycycline to induce TACC2 expression, while the control group received no doxycycline. Tumor volume and weight were significantly reduced in the doxycycline-treated mice,

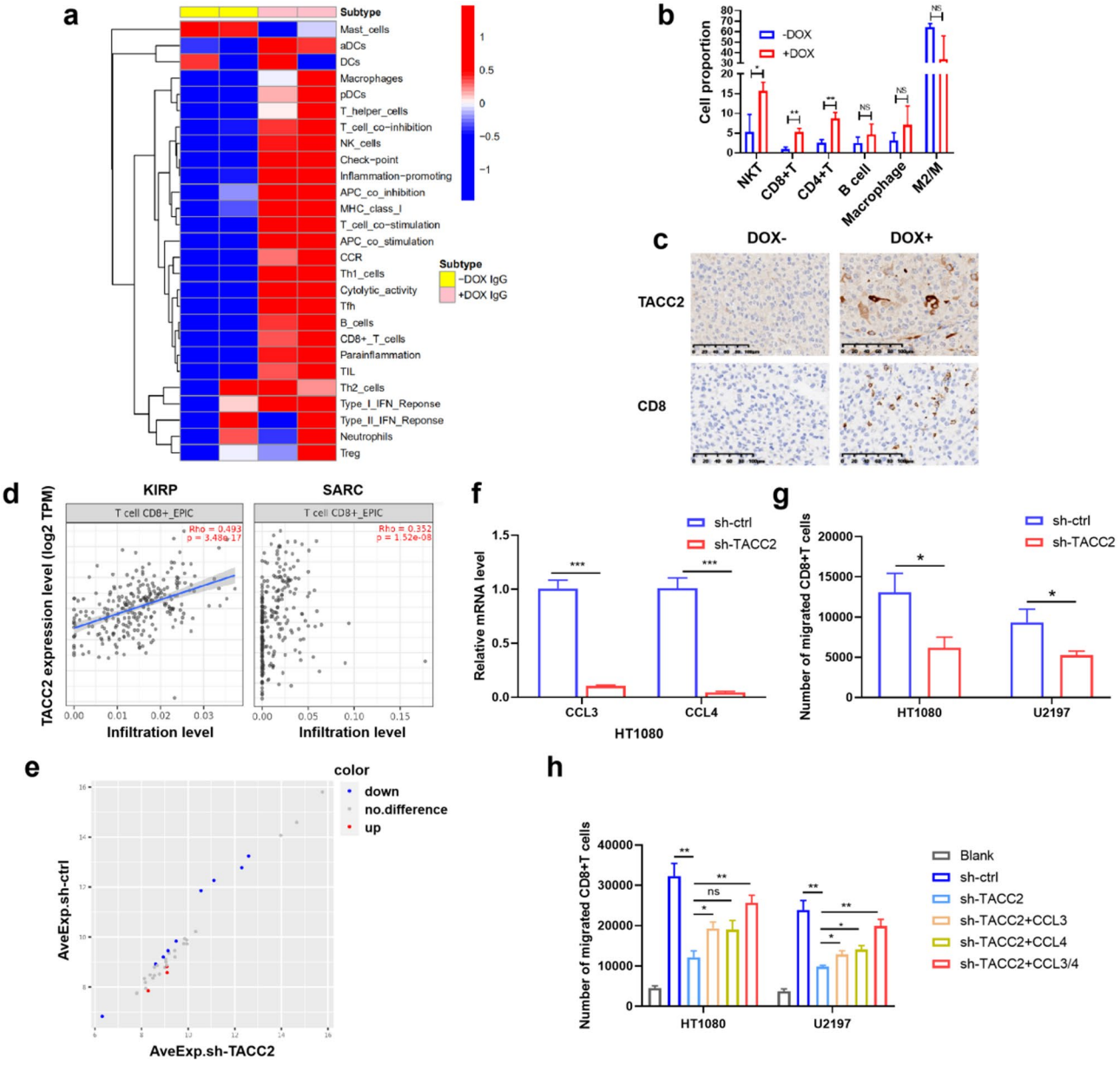

Fig. 3 (See legend on next page.)

indicating that TACC2 overexpression markedly suppressed tumor growth (Supplementary Fig. 6).

TACC2 enhances anti-tumor immunity

We conducted RNA-Seq on two groups of mouse subcutaneous tumors and performed ssGSEA analysis to assess immune cell infiltration. The results indicated that tumors in the TACC2 high expression group exhibited significantly higher infiltration levels of multiple immune cells compared to the TACC2 low expression group (Fig. 3A). Flow cytometry analysis further confirmed increased infiltration of NKT, CD8 + T, and CD4 + T cells in tumors with high TACC2 expression. No significant changes were observed in B cell or macrophage infiltration levels (Fig. 3B). Gating strategies for immune cell subset identification were detailed in Supplementary Fig. 7. Additionally, IHC staining validated that high TACC2 expression was associated with more abundant CD8 + T cell infiltration (Fig. 3C). Based on these findings, we hypothesized that TACC2 participates in immune regulation, and that higher TACC2 expression correlates with enhanced anti-tumor immunity. To test this hypothesis, we performed immune infiltration analysis using TIMER2.0 on RNA-seq data from a subset of patients in the TCGA database. These results revealed

(See figure on previous page.)

Fig. 3 TACC2 enhances the chemotaxis of CD8 + T cells by upregulating chemokines CCL3/CCL4. **a**. RNA sequencing was performed on mouse subcutaneous tumors, and single-sample Gene Set Enrichment Analysis (ssGSEA) was used to calculate an enrichment score for relative abundance of each immune cell type. **b**. Tumor-infiltrating immune cells were quantified by flow cytometry using fluorescently labeled antibodies targeting murine CD3, CD4, CD8α, NK1.1, F4/80, CD11b, CD206, and CD19. Tumors with high TACC2 expression exhibited significantly increased infiltration of NKT cells ($p = 0.0208$), CD8 + T cells ($p = 0.0025$), and CD4 + T cells ($p = 0.0035$) compared to low-expressing tumors (Student's t-test). Data are presented as the mean ± SEM ($n = 3$ mice). **c**. Immunohistochemical (IHC) staining of TACC2 and CD8 in mouse tumors. Representative images of tumors with low and high TACC2 expression (scale bar: 100 μm). **d**. Immune infiltration analysis was performed on RNA-seq data from a subset of patients in the TCGA database using TIMER2.0. Representative results from the KIRP and SARC cohorts are shown. **e**. The expression levels of 38 chemokines in the supernatant of HT1080 and U2197 cells (sh-ctrl vs. sh-TACC2) were detected using a human chemokine array. Blue dots represent chemokines downregulated after TACC2 knockdown, while red dots indicate upregulated chemokines. **f**. qRT-PCR validation of CCL3 and CCL4 mRNA levels after TACC2 knockdown in HT1080 cell line. Data are presented as the mean ± SEM ($n = 3$, Student's t-test). Experiments were performed in biological triplicates. **g**. A total of 5×10^5 CD8 + T cells isolated from healthy donors via magnetic bead sorting were added to the upper chamber of a Transwell, with supernatant from HT1080 cells or U2197 cells (sh-ctrl vs. sh-TACC2) added to the lower chamber. After 6–8 h, the cells in the lower chamber were counted. TACC2 knockdown significantly reduced CD8 + T cells migration compared to controls ($n = 3$, Student's t-test, $p = 0.004$). Data are presented as the mean ± SEM. Experiments were performed in biological triplicates. **h**. A total of 5×10^5 CD8 + T cells isolated form healthy donors via magnetic bead sorting were added to the upper chamber of a Transwell. The lower chamber contained RPMI 1640 medium, sh-ctrl HT1080 supernatant, sh-TACC2 supernatant, or sh-TACC2 supernatant supplemented with CCL3, CCL4, or a combination of CCL3/CCL4 (100 ng/mL). After 6–8 h, migrated CD8 + T cells in the lower chamber were counted. TACC2 knockdown significantly impaired the chemotactic effect of tumor cell supernatants on CD8 + T cells. This effect was partially rescued by the addition of either CCL3 or CCL4 alone, while the combined supplementation of CCL3 and CCL4 resulted in a more pronounced recovery. Data are presented as the mean ± SEM from three independent technical replicates. Experiments were performed in biological triplicates. $^{****}p < 0.0001$, $^{***}p < 0.001$, $^{**}p < 0.01$, $^{*}p < 0.05$

a positive correlation between TACC2 expression and CD8 + T cell infiltration levels (Fig. 3D).

TACC2 enhances anti-tumor immunity by upregulating chemokines CCL3/CCL4

To investigate the role of TACC2 in enhancing anti-tumor immunity, we first utilized a chemokine array to detect the expression levels of 38 common secreted chemokines. Supernatants were collected and concentrated from TACC2 knockdown (sh-TACC2) and control (sh-ctrl) HT1080 and U2197 cell lines. Knockdown of TACC2 resulted in the downregulation of nine chemokines and upregulation of three, with CCL3 and CCL4 showing the most marked decreases (Fig. 3E, Additional file 2). These findings were confirmed by qPCR, which showed significant transcriptional downregulation of CCL3 and CCL4 upon TACC2 silencing (Fig. 3F, Supplementary Fig. 8A).

To further clarify the chemotactic effect of TACC2, we conducted chemotaxis assays using peripheral blood mononuclear cells (PBMCs), CD4 + T cells, or CD8 + T cells collected from healthy donors. The upper chamber contained PBMCs, CD4 + T cells, or CD8 + T cells, while the lower chamber was filled with either normal culture medium or tumor cell supernatants, with or without recombinant CCL3 and/or CCL4 supplementation (Supplementary Fig. 8B). In the initial assay, PBMCs were placed in the upper chamber, while supernatants from HT1080 and U2197 cells transduced with either sh-TACC2 or sh-ctrl were added to the lower chamber. After 6–8 h, migrated NKT cells in the lower chamber were quantified by flow cytometry (Supplementary Fig. 8C). A decreasing trend in NKT cell migration was observed in the sh-TACC2 group; however, the difference did not reach statistical significance (Supplementary Fig. 8D).

Next, $CD4^+$ and $CD8^+$ T cells were magnetically sorted and evaluated in the same system. While $CD4^+$ T cells exhibited a decreasing trend in migration, the change was not statistically significant (Supplementary Fig. 8E). CD8 + T cell migration was significantly reduced following TACC2 knockdown, indicating a critical role of TACC2 in promoting CD8 + T cell chemotaxis (Fig. 3G). To determine whether CCL3 and CCL4 mediate this effect, rescue experiments were conducted. CD8 + T cells were placed in the upper chamber, and the lower chamber contained either normal medium, sh-ctrl supernatant, sh-TACC2 supernatant, or sh-TACC2 supernatant supplemented with recombinant CCL3, CCL4, or both. The addition of either chemokine alone partially restored CD8 + T cell migration, while combined supplementation of CCL3 and CCL4 resulted in a more robust recovery (Fig. 3H).

CCL3/CCL4 are target genes of TACC2 and depend on the NuRD/CoREST complex

In a previous study of our group, we transfected 293T cells with either EGFP or EGFP-TACC2 and performed immunoprecipitation using an EGFP antibody [23]. Mass spectrometry analysis of the immunoprecipitated proteins revealed key components of several HDAC-corepressor complexes, including SIN3A from the SIN3A complex, MTA1/2-MBD3 from the NuRD complex, and HMG20B-RCOR1-LSD1 from the CoREST complex. Class I HDACs, known for their potent deacetylase activity, play a crucial role in the deacetylation process. These complexes, together with Class I HDACs, are integral to the regulation of chromatin acetylation and transcriptional repression [24–27].

Endogenous immunoprecipitation further confirmed strong interactions between TACC2 and essential components of the HDAC complexes, such as MTA1/2, MBD3, and HMG20B (Fig. 4A). The HDAC-corepressor complexes predominantly localize in the nucleus, where

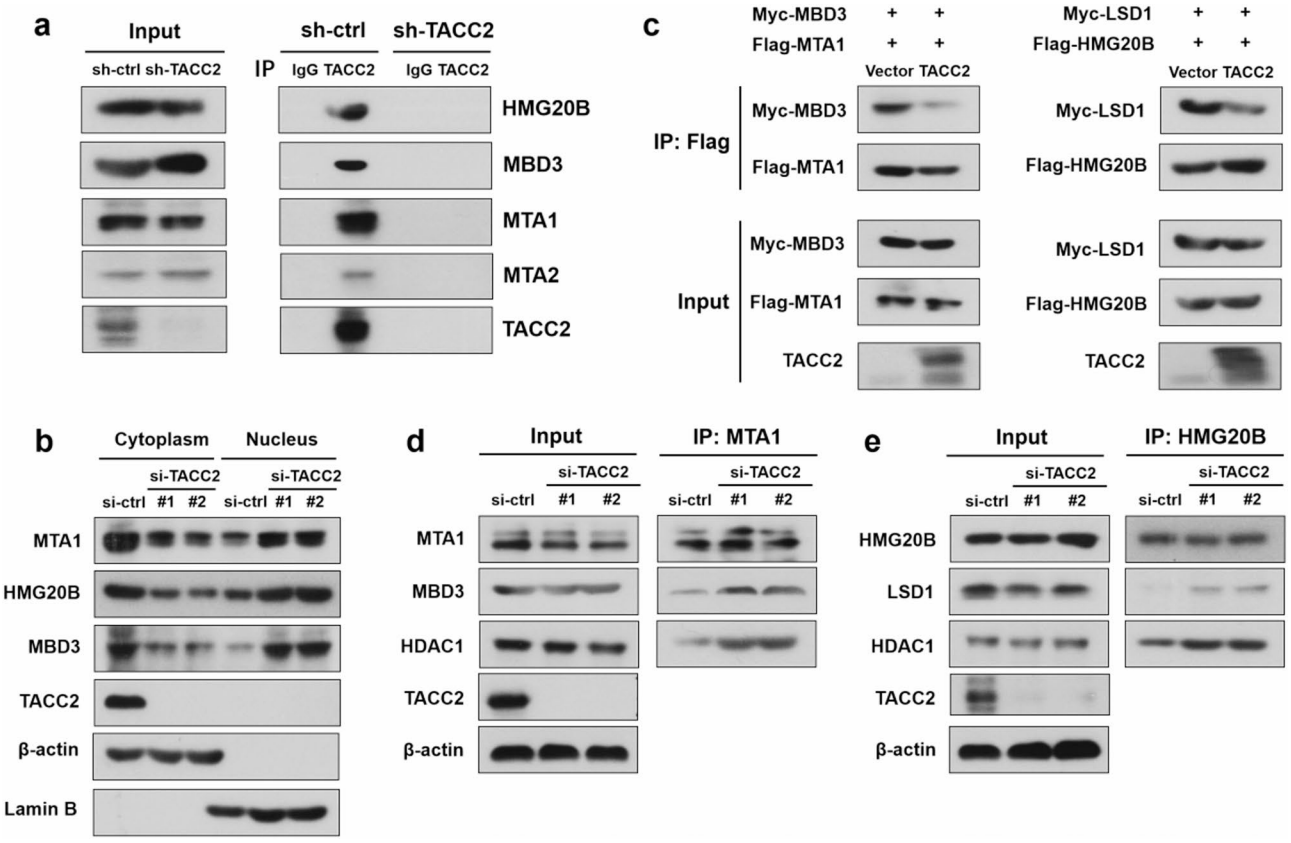

Fig. 4 TACC2 interacts with NuRD and CoREST corepressor complexes and inhibits their nuclear translocation. (**a**) Immunoprecipitation was performed to assess the interaction of TACC2 with components of the NuRD (MTA1, MTA2) and CoREST (HMG20B, LSD1) complexes in HT1080 cells. Lysates were immunoprecipitated with anti-TACC2 antibody, followed by Western blot analysis using antibodies against HMG20B, MBD3, MTA1, and MTA2. IgG was used as a negative control. Strong interactions between TACC2 and both the NuRD and CoREST complexes were observed. **b**. After HT1080 cells were transfected with either si-ctrl or TACC2 siRNA for 48 h, cytoplasmic and nuclear proteins were separated, and their expression was detected by Western blot. Lamin B (nuclear marker) and β-actin (cytoplasmic marker) confirmed the purity of the fractionation. TACC2 knockdown led to a decrease in the cytoplasmic distribution and an increase in the nuclear distribution of MTA1, MBD3, and HMG20B. **c**. 293T cells were transfected with EGFP or EGFP-TACC2 along with Flag-MTA1/ Myc-MBD3 or Flag-HMG20B / Myc-LSD1. Lysates were immunoprecipitated with anti-Flag magnetic beads, followed by Western blot analysis. Overexpression of TACC2 disrupted the interactions between MTA1 and MBD3, as well as between HMG20B and LSD1. **d** and **e**. HT1080 cells were transfected with si-ctrl or si-TACC2 for 48 h, followed by immunoprecipitation and Western blot analysis using the appropriate antibodies. siRNA-mediated knockdown of TACC2 enhanced the interactions between MTA1 and MBD3/HDAC1, as well as between HMG20B and LSD1/HDAC1. Each experiment was conducted with at least two independent biological replicates

they are involved in chromatin remodeling and transcriptional regulation [28]. Upon siRNA-mediated knockdown of TACC2 in HT1080 cells, we isolated nuclear and cytoplasmic proteins and assessed the distribution of MTA1, MBD3, and HMG20B via Western Blot. The results indicated that TACC2 knockdown led to a decrease in the cytoplasmic distribution and an increase in the nuclear distribution of MTA1, MBD3, and HMG20B (Fig. 4B).

We then explored whether the interaction between TACC2 and these proteins interfered with the formation of the HDAC-corepressor complexes. The results showed that exogenous overexpression of TACC2 disrupted interactions between MTA1 and MBD3, as well as between HMG20B and LSD1 (Fig. 4C). Conversely, siRNA-mediated knockdown of TACC2 enhanced the interactions between MTA1 and MBD3 or HDAC1, as well as between HMG20B and LSD1 or HDAC1 (Fig. 4D and E). These findings suggested that TACC2 may inhibit the nuclear translocation and functional assembly of the NuRD/CoREST complexes, thereby preventing the formation of active HDAC-corepressor complexes, which could lead to the transcriptional upregulation of CCL3 and CCL4.

Therefore, to further investigate the regulatory role of TACC2 on CCL3 and CCL4 expression, we treated TACC2 knockdown HT1080 cells and their control cells with siRNAs targeting MTA1 or HMG20B. After treatment, RNA was extracted, and qPCR was performed to measure the expression levels of CCL3 and CCL4. The results showed that the knockdown of MTA1 or HMG20B partially rescued the reduction in CCL3 and CCL4 expression caused by TACC2 deficiency (Fig. 5A

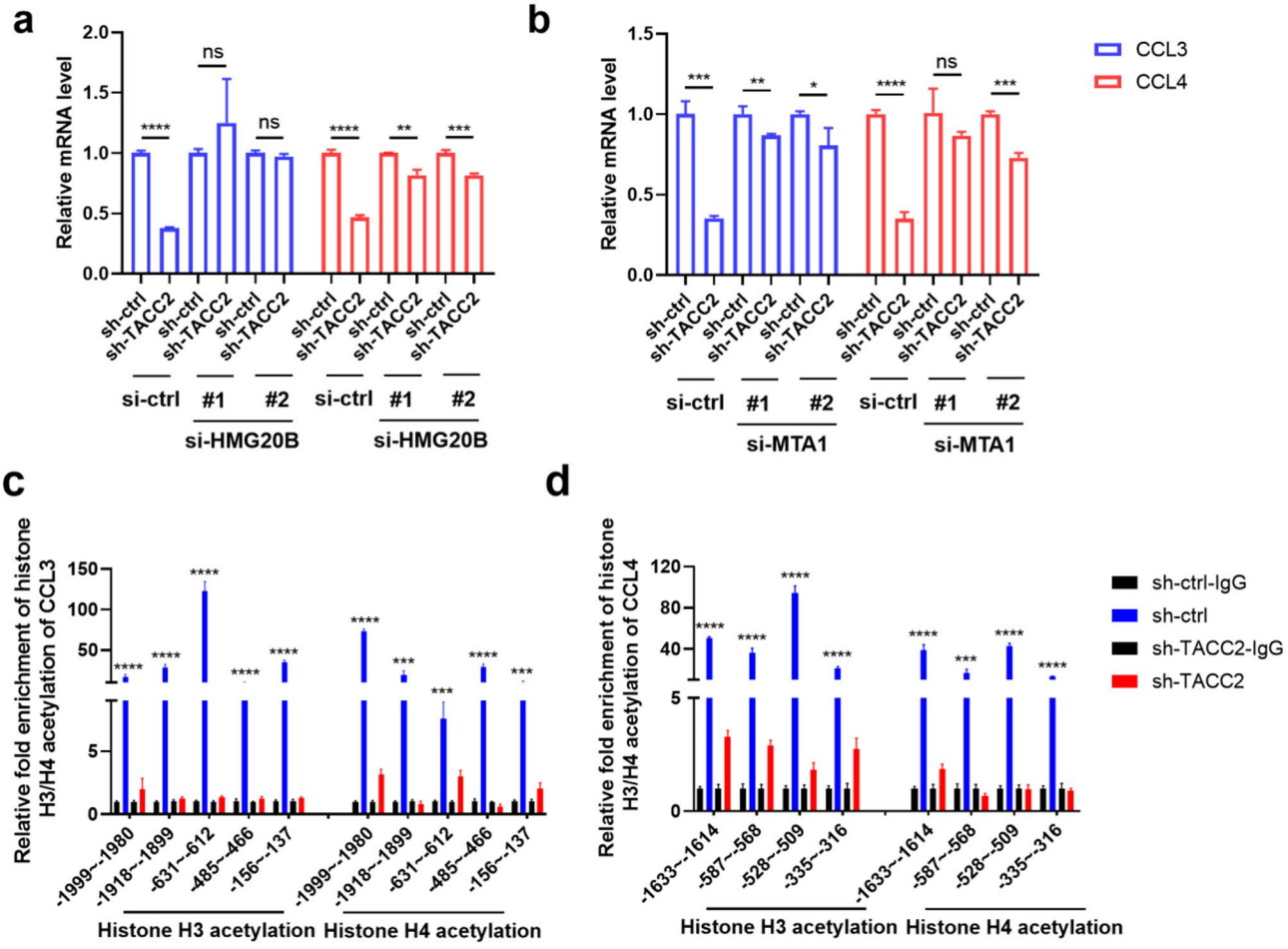

Fig. 5 TACC2 regulates CCL3/CCL4 expression via NuRD/CoREST complex-mediated epigenetic modulation. **a**,**b**. HT1080 cells were transduced with control shRNA (sh-ctrl) or TACC2-targeting shRNA (sh-TACC2), followed by siRNA-mediated knockdown of HMG20B (**a**) or MTA1 (**b**). After 48 h, CCL3 and CCL4 mRNA levels were measured by qRT-PCR. Silencing of TACC2 reduced the expression of CCL3 and CCL4, which was partially rescued by HMG20B or MTA1 knockdown (mean ± SD, $n = 3$; Student's t-test; $^{**}p < 0.01$, $^{***}p < 0.001$, $^{****}p < 0.0001$). Experiments were performed in biological triplicates. **c**, **d**. Chromatin immunoprecipitation (ChIP)-qPCR analysis was performed to assess histone H3K27ac (**c**) and H4K16ac (**d**) enrichment at the CCL3 and CCL4 promoter regions in sh-ctrl and sh-TACC2 HT1080 cells. Immunoprecipitated DNA was normalized to input and quantified relative to IgG controls. TACC2 knockdown led to a marked decrease in H3K27ac and H4K16ac acetylation at both promoters, indicating enhanced chromatin condensation and transcriptional repression. Data are presented as the mean ± SD ($n = 3$, Student's t-test; $^{***}p < 0.001$, $^{****}p < 0.0001$). Experiments were performed in biological triplicates

and B). Finally, to confirm the role of TACC2 in the transcriptional activation of CCL3/CCL4 through chromatin acetylation, we performed ChIP-qPCR analysis. The results demonstrated a significant reduction in H3 and H4 acetylation levels at the CCL3/CCL4 promoter regions following TACC2 silencing (Figs. 5C-D). Collectively, these findings demonstrated that TACC2 depletion promoted the epigenetic repression of CCL3 and CCL4 by facilitating the engagement of the HDAC-corepressor complexes.

TACC2 enhances the efficacy of PD-1 antibody by upregulating immune cell infiltration

Based on the above findings, we further explored the correlation between TACC2 expression levels and the efficacy of anti-PD-1 therapy. We established a subcutaneous tumor model in mice and treated them with PD-1 antibody or isotype control antibody. The results showed that in the TET-ON system for TACC2 gene expression, the tumor weight in the anti-PD-1 therapy group was approximately 50% of that in the control group in the absence of doxycycline (DOX). Upon DOX induction to upregulate TACC2 expression, the anti-tumor effect of the PD-1 antibody was significantly enhanced, with complete regression observed in some mice (2/6, 33.3%) (Figs. 6A-C). Moreover, the survival of mice in the high TACC2 expression group treated with PD-1 antibody was significantly prolonged compared to other groups (Fig. 6D).

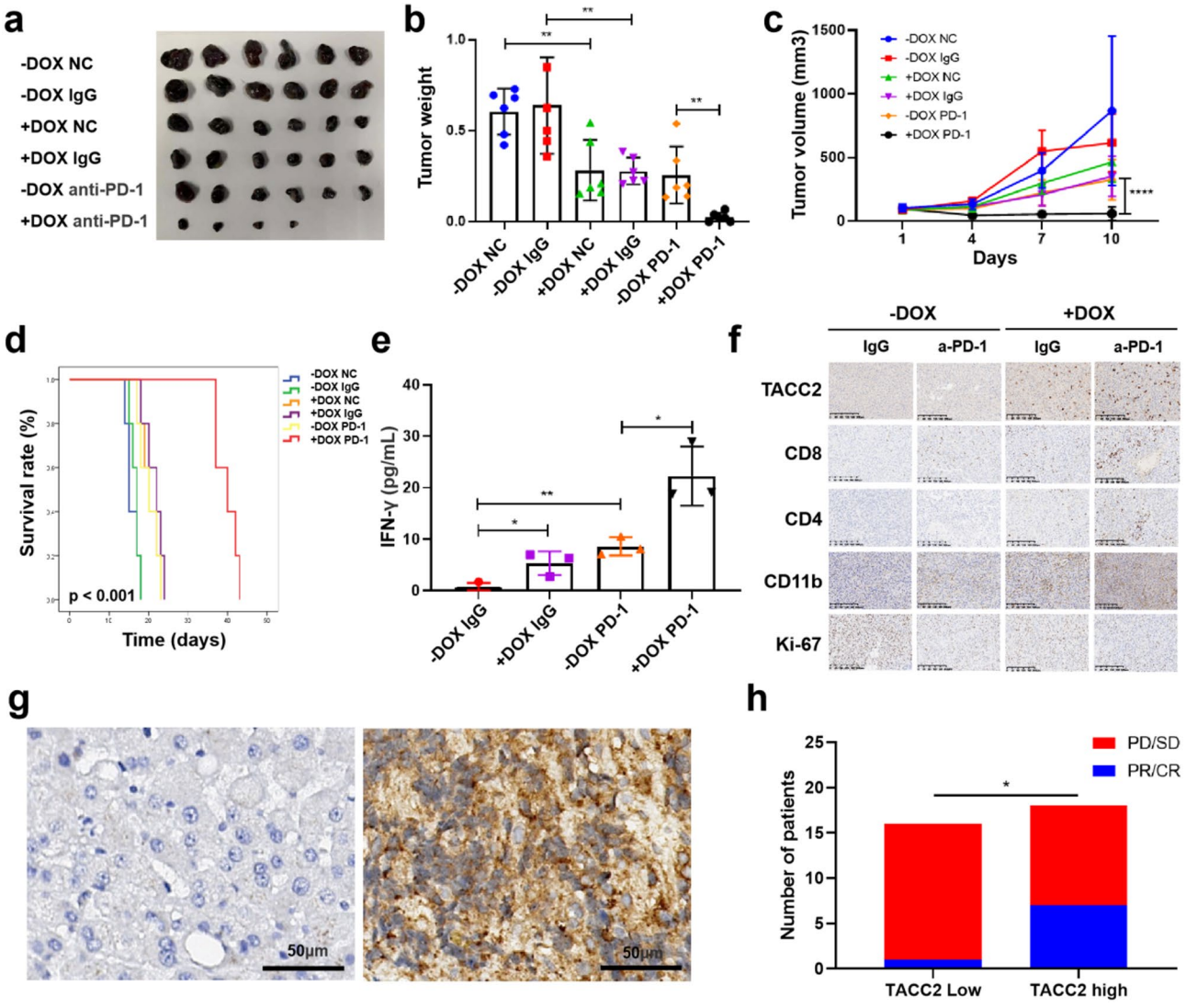

Fig. 6 The efficacy of anti-PD-1 antibody is significantly enhanced when TACC2 is highly expressed. **a**. Doxycycline-inducible TACC2 overexpressing MCA205 cells were established using Tet-on 3G system. Tumor xenograft models were established by subcutaneously injecting 5×10^5 tumor cells into the right flank of female C57BL/6 mice. Anti-PD-1 antibody (10 mg/kg, i.p. every 3 days) was administered when tumors reached approximately 100 mm^3 (6 mice/group). Body weight was monitored, and tumor dimensions were measured every three days with calipers. Upon DOX induction to upregulate TACC2 expression, the anti-tumor effect of anti-PD-1 antibody was significantly enhanced, with complete regression observed in 2/6 mice (representative tumor images shown). **b**. Weight comparison of subcutaneous tumors across different groups. Data are presented as mean ± SD. The TACC2-high expression treated with PD-1 antibody group exhibited the smallest tumor mass (Student's t test, $^{**}p < 0.01$). **c**. Tumor volume growth curves, with volume calculated as 0.52 × tumor length × tumor $width^2$. Data are presented as mean ± SD (Student's t test, $^{**}p < 0.01$). **d**. Survival curve of mice in each group. The TACC2-high expression treated with PD-1 antibody group exhibited prolonged survival (Log-rank test, $p < 0.001$). **e**. Serum IFN-γ levels of mice in each group were detected by ELISA. Mice in the TACC2-high expression treated with PD-1 antibody group exhibited the highest levels of IFN-γ (mean ± SD; Student's t test, $^{*}p < 0.05$, $^{**}p < 0.01$). **f**. Immunohistochemical (IHC) staining for TACC2, CD4, CD8, CD11b, and Ki-67 was performed on mouse subcutaneous tumors. Representative images were presented. Scale bar: 100 μm. **g**. IHC staining of TACC2 was performed on the tumor tissues from sarcoma patients treated with PD-1 antibody. The proportion of positively stained cells was quantified (1–25% = 1, 26–50% = 2, 51–75% = 3, 76–100% = 4), and staining intensity was scored (negative = 0, weak = 1, moderate = 2, strong = 3). The total score was calculated as the product of the positive rate and intensity scores, with 0–5 indicating low expression and 6–12 indicating high expression. Representative images of high and low TACC2 expression are shown. Scale bars: 100 μm. **h**. The efficacy of anti-PD-1 antibody in sarcoma patients with high and low expression of TACC2 were evaluated. Efficacy endpoints include progressive disease/stable disease (PD/SD) and partial/complete response (PR/CR). High TACC2 expression correlated with higher PR/CR rates (Fisher's exact test, $^{*}p = 0.0408$). Red, PD/SD; blue, PR/CR

We measured the levels of interferon-gamma (IFN-γ) in the peripheral blood serum of the mice and found that the group with high TACC2 expression treated with PD-1 antibody exhibited the highest levels of IFN-γ (Fig. 6E). Immunohistochemical staining of the subcutaneous tumor tissues revealed that CD8 + T and CD4 + T cell infiltration was more abundant in the high TACC2 expression group compared to the low TACC2 expression group. Furthermore, immune cell infiltration in subcutaneous tumor was significantly enhanced in PD-1 antibody-treated mice of high TACC2 expression group compared to the other groups (Fig. 6F).

To validate these findings in a clinical setting, we collected tissue samples from 34 sarcoma patients who received PD-1 antibody treatment at our center and performed TACC2 immunohistochemical staining on the tissue sections. TACC2 expression in tumor tissues was scored based on staining intensity and positivity rate. The staining intensity was scored as follows: 0 (negative), 1 (1+), 2 (2+), and 3 (3+). while the staining positivity rate was scored as: 0 (negative), 1 (1–25%), 2 (26–50%), 3 (51–75%), and 4 (76–100%). The total score for each patient was calculated by multiplying the intensity and positivity scores, with a score of 0–5 classified as the low expression group and a score of 6–12 classified as the high expression group (Fig. 6G). Among 34 sarcoma patients receiving anti-PD-1 therapy, high TACC2 expression was associated with enhanced therapeutic efficacy. In the TACC2-low group ($n = 16$), 93.8% (15/16) exhibited a best therapeutic response of PD/SD, with only 6.3% (1/16) achieving PR/CR. In contrast, the TACC2-high cohort ($n = 18$) showed significantly improved outcomes, with 38.9% (7/18) PR/CR and an overall response rate (ORR) of 38.9% versus 6.3%. Subtype-specific analysis revealed varied response patterns: liposarcoma demonstrated 66.7% ORR (2/3 PR/CR) exclusively in TACC2-high patients; osteosarcoma showed 50% ORR (1/2 PR/CR) in TACC2-high versus 0% (0/5) in TACC2-low; and other subtypes ($n = 11$) exhibited 50% ORR (4/8) in TACC2-high versus 0% (0/3) in TACC2-low (Supplementary Fig. 9). These findings suggested that TACC2 expression may serve as a predictive biomarker for response to PD-1 blockade in sarcomas. However, given the limited sample size within each histological subtype in our cohort, further validation in larger, subtype-stratified studies is warranted to confirm these observations.

Discussion

STS, though rare, is a highly aggressive and clinically challenging malignancy, characterized by its propensity for recurrence, metastasis, and typically poor prognosis. Tumor suppressor genes are central to the prevention, diagnosis, treatment, and prognosis of STS, and the discovery of novel tumor suppressors could provide vital insights into more effective therapeutic strategies [29]. While PD-1 inhibitors have emerged as a promising treatment option for various cancers, their efficacy in STS has been largely suboptimal, with the majority of patients either showing limited benefit or even experiencing hyperprogression [10, 30, 31]. This highlights an urgent need for reliable biomarkers to predict treatment response and guide therapeutic decisions in STS. In this study, we provided evidence supporting the role of TACC2 as a novel tumor suppressor in STS, offering fresh insights into its potential as a predictive biomarker and therapeutic target.

TACC2, a member of the TACC protein family, is primarily known for its role in microtubule formation and mitotic spindle stabilization, crucial for maintaining chromosomal stability. Abnormal TACC2 expression can disrupt chromatin remodeling complexes, leading to genomic instability and tumorigenesis. Previous studies have suggested that TACC2 acts as a tumor suppressor in breast cancer, where its expression is significantly reduced in tumor cells compared to non-cancerous cells [32]. However, its role in other cancers, such as prostate and liver cancers, has been more controversial, with some reports suggesting tumor-promoting activities [22, 33, 34]. In the context of STS, our study is the first to report that TACC2 expression was significantly lower in STS tumor tissues compared to normal tissues, and reduced TACC2 expression correlated with poor prognosis, particularly in terms of OS. However, the correlation between TACC2 expression and PFS did not reach statistical significance.The lack of a significant correlation may be due to several factors. PFS is influenced by tumor response to therapy and progression dynamics, which can be heterogeneous. Additionally, the diverse treatment regimens among patients may impact PFS outcomes, further complicating this relationship. These factors could overshadow the effect of TACC2 on short-term tumor progression, with its influence on survival becoming more evident over time.

The tumor microenvironment plays a critical role in tumor progression and response to therapy, with immune cells being key players in this process. Tumor cells secrete a variety of cytokines, chemokines, and other factors, which can recruit immune cells to the tumor site and shape the immune landscape [35, 36]. Among these, chemokines such as CCL2, CCL3, CCL4, CCL5, CXCL9, and CXCL10 have been reported to be significantly correlated with the levels of tumor-infiltrating lymphocytes (TILs). For example, the upregulation of CCL3 and CCL20 by RUNX3 has been shown to promote CD8 + T cell recruitment in lung cancer [37]. Macrophage inflammatory protein (MIP)-1 mainly includes CCL3 (MIP-1α), CCL4 (MIP-1β), and CCL5 (RANTES). MIP-1 has been shown to be a major determinant of immune cell infiltration in

certain tumors by directly recruiting antigen-presenting cells, including dendritic cells, to the tumor site, thereby recruiting T cells into the tumor microenvironment [38]. Similarly, CCL4 has been reported to be positively correlated with TILs infiltration in melanoma [39]. By combining bioinformatics analysis with in vitro and in vivo experiments, we uncovered the pivotal role of TACC2 in regulating the tumor immune microenvironment. We found that TACC2 enhances immune cell infiltration through its upregulation of CCL3 and CCL4, which play a pivotal role in recruiting immune cells into the tumor microenvironment. Specifically, we observed that TACC2 knockdown in HT1080 and U2197 cells reduced the chemotaxis of CD8 + T cells, while supplementation with CCL3 and CCL4 partially restored this effect, emphasizing the critical role of TACC2 in immune cell recruitment.

Histone acetylation, regulated by histone acetyltransferases (HATs) and HDACs, is crucial for gene expression regulation [40, 41]. HDACs, through their catalytic subunits in multi-protein complexes, promote chromatin condensation and are closely associated with gene transcriptional repression [42]. In mammals, Class I HDACs are typically found in four types of multiprotein complexes: the CoREST complex, the MTA1/NuRD complex, the NcoR/SMRT complex, and the SIN3A complex. These complexes localize HDACs to specific genomic regions, where they mediate transcriptional repression. At the molecular level, our study, consistent with previous research, observed the interaction between TACC2 and the NuRD/CoREST complex, a key chromatin-remodeling complex involved in gene silencing [23]. TACC2 inhibited the nuclear translocation of this complex, thereby preventing the formation of transcriptionally repressive HDAC-corepressor complexes. This, in turn, facilitated the transcription of CCL3 and CCL4, promoting immune cell infiltration and enhancing the anti-tumor immune response. Interestingly, previous studies have also highlighted TACC2's interaction with various histone acetyltransferases, including PCAF, hGCN5L2, and p300/cbp, suggesting that TACC2 may play a broader role in chromatin remodeling and gene activation [43]. These findings open new avenues for exploring the regulatory functions of TACC2 in chromatin dynamics and its potential as a therapeutic target for enhancing immune responses.

While our findings suggest that TACC2 may serve as a prognostic marker and modulator of the immune microenvironment in STS, several limitations should be acknowledged. First, the small sample size of the anti-PD-1-treated cohort ($n = 34$), especially the limited representation within individual histological subtypes, restricts the statistical power of subtype-specific analyses and underscores the need for validation in larger, histology-stratified cohorts. Second, while flow cytometry revealed increased infiltration of NKT, CD4 + T, and CD8 + T cells in TACC2-high tumors, our functional studies focused primarily on CD8 + T cells due to their established role in anti-tumor immunity. Future studies should explore the contributions of other immune subsets to TACC2-mediated immune modulation. Third, the retrospective design and treatment heterogeneity may introduce bias, highlighting the necessity for prospective trials with histology-specific enrollment.

Conclusions

In conclusion, our study identifies TACC2 as a critical tumor suppressor in STS, with significant implications for prognosis and immune regulation. We demonstrate that TACC2 plays a critical role in modulating the tumor immune microenvironment, in part by promoting chemokine-mediated recruitment of immune effector cells. Notably, higher TACC2 expression was associated with improved response rates to PD-1 antibody therapy in a retrospective sarcoma cohort, suggesting its potential as a predictive biomarker for immune checkpoint blockade. These findings provide new insights into the immunomodulatory functions of TACC2 and raise the possibility that it may serve as a clinically relevant marker for patient stratification in immunotherapy. However, further validation in larger, histology-stratified prospective cohorts is essential to fully establish its predictive utility and therapeutic relevance.

Abbreviations

STS	Soft tissue sarcoma
OS	Overall survival
PFS	Progression-free survival
PD-1	Programmed death-1
PD-L1	Programmed death ligand-1
NCCN	National Comprehensive Cancer Network
TACCs	Transforming acidic coiled-coil proteins
WES	Whole-exome sequencing
CNV	Copy number variation
PBMCs	Peripheral blood mononuclear cells
DOX	Doxycycline
IFN-γ	Interferon-gamma
ORR	Overall response rate
TILs	Tumor-infiltrating lymphocytes
MIP-1	Macrophage inflammatory protein-1
IHC	Immunohistochemistry
qRT-PCR	Quantitative real-time PCR
ELISA	Enzyme-linked immunosorbent assay
ssGSEA	Single-sample Gene Set Enrichment Analysis

Supplementary Information

The online version contains supplementary material available at https://doi.org/10.1186/s12943-025-02354-2.

Supplementary Material 1

Supplementary Material 2

Supplementary Material 3

Supplementary Material 4

Acknowledgements
Not applicable.

Author contributions
Study concept and design: Xing Zhang, Jing Yang, Tianliang Xia. Development of methodology: Jing Yang, Xiaxia Lu, Qiyan Cai, Tianliang Xia, Mengmeng Liu. Acquisition, analysis or interpretation of data: Jing Yang, Xiuxia Lu, Qiyan Cai, Mengmeng Liu, Liyuan Le. Manuscript preparation: Jing Yang, Xiuxia Lu. Manuscript editing: Xing Zhang. Technical or material support: Xinke Zhang. All authors have read and approved the article, and agree to be accountable for all aspects of this work.

Funding
This work was supported by the the National Natural Science Foundation of China (No. 82203523, 82072958, and 82272699), National Key Research and Development Program of China (No. 2021YFC2400600/2021YFC2400601), and the Guangzhou Basic and Applied Basic Research Foundation of Science and Technology Projects (No. 2023A04J2140).

Data availability
Data is provided within the manuscript or supplementary information files.

Declarations

Ethics approval and consent to participate
The study was approved by the Institutional Review Board of Sun Yat-Sen University Cancer Center (Approve number: G2023-128-01).

Consent for publication
Not applicable.

Competing interests
The authors declare no competing interests.

Author details
[1]Melanoma and Sarcoma Medical Oncology Unit, State Key Laboratory of Oncology in South China, Sun Yat-sen University Cancer Center, Guangzhou 510060, P.R. China
[2]Department of Radiology, State Key Laboratory of Oncology in South China, Guangdong Provincial Clinical Research Center for Cancer, Collaborative Innovation Center for Cancer Medicine, Sun Yat-sen University Cancer Center, Guangzhou, Guangdong, P.R. China
[3]Department of Oncology, The Second Affiliated Hospital, Jiangxi Medical College, Jiangxi Key Laboratory of Clinical Translational Cancer Research, Nanchang University, Nanchang, Jiangxi 330000, P.R. China
[4]State Key Laboratory of Oncology in South China, Guangdong Provincial Clinical Research Center for Cancer, Sun Yat-sen University Cancer Center, Guangzhou 510060, P.R. China
[5]Department of Nuclear Medicine, State Key Laboratory of Oncology in South China, Collaborative Innovation Center of Cancer Medicine, Sun Yat-Sen University Cancer Center, 651 Dongfeng Road East, Guangzhou 510060, Guangdong, People's Republic of China
[6]State Key Laboratory of Oncology in South China, Collaborative Innovation Center for Cancer Medicine, Department of Pathology, Sun Yat-sen University Cancer Center, Guangzhou, China

Received: 17 February 2025 / Accepted: 14 May 2025
Published online: 30 May 2025

References

1. Andritsch E, Beishon M, Bielack S, Bonvalot S, Casali P, Crul M, Delgado Bolton R, Donati DM, Douis H, Haas R, et al. ECCO essential requirements for quality Cancer care: soft tissue sarcoma in adults and bone sarcoma. A critical review. Crit Rev Oncol Hematol. 2017;110:94–105.
2. von Mehren M, Randall RL, Benjamin RS, Boles S, Bui MM, Ganjoo KN, George S, Gonzalez RJ, Heslin MJ, Kane JM, et al. Soft tissue sarcoma, version 2.2018, NCCN clinical practice guidelines in oncology. J Natl Compr Canc Netw. 2018;16:536–63.
3. Siegel RL, Giaquinto AN, Jemal A. Cancer statistics, 2024. CA Cancer J Clin. 2024;74:12–49.
4. Kallen ME, Hornick JL. The 2020 WHO classification: what's new in soft tissue tumor pathology?? Am J Surg Pathol. 2021;45:e1–23.
5. Subramanian A, Nemat-Gorgani N, Ellis-Caleo TJ, van Sears IDGP, Somani TJ, Luca A, Zhou BA, Bradic MY, Torres M. Sarcoma microenvironment cell States and ecosystems are associated with prognosis and predict response to immunotherapy. Nat Cancer. 2024;5:642–58.
6. Judson I, Verweij J, Gelderblom H, Hartmann JT, Schöffski P, Blay JY, Kerst JM, Sufliarsky J, Whelan J, Hohenberger P, et al. Doxorubicin alone versus intensified doxorubicin plus Ifosfamide for first-line treatment of advanced or metastatic soft-tissue sarcoma: a randomised controlled phase 3 trial. Lancet Oncol. 2014;15:415–23.
7. Ryan CW, Merimsky O, Agulnik M, Blay JY, Schuetze SM, Van Tine BA, Jones RL, Elias AD, Choy E, Alcindor T, et al. PICASSO III: A phase III, Placebo-Controlled study of doxorubicin with or without Palifosfamide in patients with metastatic soft tissue sarcoma. J Clin Oncol. 2016;34:3898–905.
8. Tap WD, Papai Z, Van Tine BA, Attia S, Ganjoo KN, Jones RL, Schuetze S, Reed D, Chawla SP, Riedel RF, et al. Doxorubicin plus Evofosfamide versus doxorubicin alone in locally advanced, unresectable or metastatic soft-tissue sarcoma (TH CR-406/SARC021): an international, multicentre, open-label, randomised phase 3 trial. Lancet Oncol. 2017;18:1089–103.
9. Petitprez F, de Reyniès A, Keung EZ, Chen TW, Sun CM, Calderaro J, Jeng YM, Hsiao LP, Lacroix L, Bougoüin A, et al. B cells are associated with survival and immunotherapy response in sarcoma. Nature. 2020;577:556–60.
10. Tawbi HA, Burgess M, Bolejack V, Van Tine BA, Schuetze SM, Hu J, D'Angelo S, Attia S, Riedel RF, Priebat DA, et al. Pembrolizumab in advanced soft-tissue sarcoma and bone sarcoma (SARC028): a multicentre, two-cohort, single-arm, open-label, phase 2 trial. Lancet Oncol. 2017;18:1493–501.
11. Roulleaux-Dugage M, Italiano A. New immunotherapy strategies for patients with sarcomas: highlights from the 2023 ASCO annual meeting. *J Hematol Oncol* 2023, 16:93.
12. Keung EZ, Burgess M, Salazar R, Parra ER, Rodrigues-Canales J, Bolejack V, Van Tine BA, Schuetze SM, Attia S, Riedel RF, et al. Correlative analyses of the SARC028 trial reveal an association between Sarcoma-Associated immune infiltrate and response to pembrolizumab. Clin Cancer Res. 2020;26:1258–66.
13. Liu Y, Hu X, Han C, Wang L, Zhang X, He X, Lu X. Targeting tumor suppressor genes for cancer therapy. BioEssays. 2015;37:1277–86.
14. Li GZ, Okada T, Kim YM, Agaram NP, Sanchez-Vega F, Shen Y, Tsubokawa N, Rios J, Martin AS, Dickson MA, et al. Rb and p53-Deficient Myxofibrosarcoma and undifferentiated pleomorphic sarcoma require Skp2 for survival. Cancer Res. 2020;80:2461–71.
15. Stefano S, Giovanni S. The PTEN tumor suppressor gene in soft tissue sarcoma. Cancers (Basel) 2019, 11.
16. Zheng C, Tang F, Min L, Hornicek F, Duan Z, Tu C. PTEN in osteosarcoma: recent advances and the therapeutic potential. Biochim Biophys Acta Rev Cancer. 2020;1874:188405.
17. Hollstein M, Sidransky D, Vogelstein B, Harris CC. p53 mutations in human cancers. Science. 1991;253:49–53.
18. Ha GH, Kim JL, Breuer EK. Transforming acidic coiled-coil proteins (TACCs) in human cancer. Cancer Lett. 2013;336:24–33.
19. Piekorz RP, Hoffmeyer A, Duntsch CD, McKay C, Nakajima H, Sexl V, Snyder L, Rehg J, Ihle JN. The centrosomal protein TACC3 is essential for hematopoietic stem cell function and genetically interfaces with p53-regulated apoptosis. Embo J. 2002;21:653–64.
20. Lauffart B, Gangisetty O, Still IH. Molecular cloning, genomic structure and interactions of the putative breast tumor suppressor TACC2. Genomics. 2003;81:192–201.
21. Onodera Y, Takagi K, Miki Y, Takayama K, Shibahara Y, Watanabe M, Ishida T, Inoue S, Sasano H, Suzuki T. TACC2 (transforming acidic coiled-coil protein 2) in breast carcinoma as a potent prognostic predictor associated with cell proliferation. Cancer Med. 2016;5:1973–82.
22. Shakya M, Zhou A, Dai D, Zhong Q, Zhou Z, Zhang Y, Li X, Bholee AK, Chen M. High expression of TACC2 in hepatocellular carcinoma is associated with poor prognosis. Cancer Biomark. 2018;22:611–9.
23. Lin ZR, Xia TL, Wang MY, Zhang LJ, Liu YM, Yuan BY, Zhou AJ, Yuan L, Zheng J, Bei JX et al. Inactivation of TACC2 epigenetically represses CDKN1A and confers sensitivity to CDK inhibitors. Med 2025:100568.
24. Seto E, Yoshida M. Erasers of histone acetylation: the histone deacetylase enzymes. Cold Spring Harb Perspect Biol. 2014;6:a018713.

25. Kelly RD, Cowley SM. The physiological roles of histone deacetylase (HDAC) 1 and 2: complex co-stars with multiple leading parts. Biochem Soc Trans. 2013;41:741–9.
26. Asmamaw MD, He A, Zhang LR, Liu HM, Gao Y. Histone deacetylase complexes: structure, regulation and function. Biochim Biophys Acta Rev Cancer. 2024;1879:189150.
27. Grimes JA, Nielsen SJ, Battaglioli E, Miska EA, Speh JC, Berry DL, Atouf F, Holdener BC, Mandel G, Kouzarides T. The co-repressor mSin3A is a functional component of the REST-CoREST repressor complex. J Biol Chem. 2000;275:9461–7.
28. Latypova X, Vincent M, Mollé A, Adebambo OA, Fourgeux C, Khan TN, Caro A, Rosello M, Orellana C, Niyazov D, et al. Haploinsufficiency of the Sin3/HDAC corepressor complex member SIN3B causes a syndromic intellectual disability/autism spectrum disorder. Am J Hum Genet. 2021;108:929–41.
29. Weinberg RA. Oncogenes and tumor suppressor genes. CA Cancer J Clin. 1994;44:160–70.
30. Klemen ND, Hwang S, Bradic M, Rosenbaum E, Dickson MA, Gounder MM, Kelly CM, Keohan ML, Movva S, Thornton KA, et al. Long-term Follow-up and patterns of response, progression, and hyperprogression in patients after PD-1 Blockade in advanced sarcoma. Clin Cancer Res. 2022;28:939–47.
31. Toulmonde M, Penel N, Adam J, Chevreau C, Blay JY, Le Cesne A, Bompas E, Piperno-Neumann S, Cousin S, Grellety T, et al. Use of PD-1 targeting, macrophage infiltration, and IDO pathway activation in sarcomas: A phase 2 clinical trial. JAMA Oncol. 2018;4:93–7.
32. Chen HM, Schmeichel KL, Mian IS, Lelièvre S, Petersen OW, Bissell MJ. AZU-1: a candidate breast tumor suppressor and biomarker for tumor progression. Mol Biol Cell. 2000;11:1357–67.
33. Cheng S, Douglas-Jones A, Yang X, Mansel RE, Jiang WG. Transforming acidic coiled-coil-containing protein 2 (TACC2) in human breast cancer, expression pattern and clinical/prognostic relevance. Cancer Genomics Proteom. 2010;7:67–73.
34. Takayama K, Horie-Inoue K, Suzuki T, Urano T, Ikeda K, Fujimura T, Takahashi S, Homma Y, Ouchi Y, Inoue S. TACC2 is an androgen-responsive cell cycle regulator promoting androgen-mediated and castration-resistant growth of prostate cancer. Mol Endocrinol. 2012;26:748–61.
35. Hinshaw DC, Shevde LA. The tumor microenvironment innately modulates Cancer progression. Cancer Res. 2019;79:4557–66.
36. de Visser KE, Joyce JA. The evolving tumor microenvironment: from cancer initiation to metastatic outgrowth. Cancer Cell. 2023;41:374–403.
37. Song Q, Shang J, Zhang C, Chen J, Zhang L, Wu X. Transcription factor RUNX3 promotes CD8(+) T cell recruitment by CCL3 and CCL20 in lung adenocarcinoma immune microenvironment. J Cell Biochem. 2020;121:3208–20.
38. Allen F, Bobanga ID, Rauhe P, Barkauskas D, Teich N, Tong C, Myers J, Huang AY. CCL3 augments tumor rejection and enhances CD8(+) T cell infiltration through NK and CD103(+) dendritic cell recruitment via IFNγ. Oncoimmunology. 2018;7:e1393598.
39. Huang B, Han W, Sheng ZF, Shen GL. Identification of immune-related biomarkers associated with tumorigenesis and prognosis in cutaneous melanoma patients. Cancer Cell Int. 2020;20:195.
40. Marks PA, Miller T, Richon VM. Histone deacetylases. Curr Opin Pharmacol. 2003;3:344–51.
41. Roth SY, Denu JM, Allis CD. Histone acetyltransferases. Annu Rev Biochem. 2001;70:81–120.
42. Minucci S, Pelicci PG. Histone deacetylase inhibitors and the promise of epigenetic (and more) treatments for cancer. Nat Rev Cancer. 2006;6:38–51.
43. Gangisetty O, Lauffart B, Sondarva GV, Chelsea DM, Still IH. The transforming acidic coiled coil proteins interact with nuclear histone acetyltransferases. Oncogene. 2004;23:2559–63.

Publisher's note